VII International Conference on Particle-Based Methods
PARTICLES 2021
P. Wriggers, M. Bischoff, E. Oñate, A. Düster & T. Zohdi (Eds)

GRAIN DEFORMABILITY INFLUENCE ON THE FRACTURE BEHAVIOUR OF ROCK

N. MONTEIRO AZEVEDO[*], M.L. BRAGA FARINHA[†]

[*] Concrete Dams Department
Laboratório Nacional de Engenharia Civil (LNEC)
Av. do Brasil 101, 1700-066 Lisboa, Portugal
e-mail: nazevedo@lnec.pt, www.lnec.pt/organizacao/dbb

[†] Concrete Dams Department
Laboratório Nacional de Engenharia Civil (LNEC)
Av. do Brasil 101, 1700-066 Lisboa, Portugal
e-mail: lbraga@lnec.pt, www.lnec.pt/organizacao/dbb

Key words: Fracture, Rock, DEM, FEM, Particle deformability.

Abstract. It is known that the initially proposed circular/spherical rigid particle models are not able to match the ratio of the compressive strength to tensile strength that occurs in rock and the predicted macroscopic friction angle was much lower than the known hard rock experimental values. For this reason, several enhancements have been proposed to address these issues, namely the use of a clumped particle logic, the increase of the number of contacts per particle, the adoption of polygonal/polyhedral grain structures. A flexible 2D DEM based particle model that allows deformable particles to interact in a simplified away is presented. The flexible particle model is tested using biaxial tests and Brazilian tests. The results obtained are compared with those obtained with a rigid particle model with similar contact strength properties and with a flexible particle model, where the flexibility is due to the inner discretization of the grain with smaller particles. The results show that the proposed flexible particle model can predict a behaviour similar to a flexible particle model through inner particle discretization that is more computationally demanding. It is also shown that when compared with a rigid model, the flexible model predicts more reasonable indirect tensile strength to direct tensile strength ratio and requires a smaller value of contact fracture energy to give a good agreement with known experimental data.

1 INTRODUCTION

Rigid particle models taking directly into consideration the physical mechanisms and the influence of the material grain structure have been developed for fracture studies of quasi-brittle material such as rock [1, 2]. Initially, the proposed circular/spherical rigid particle models were not able to match the ratio of the compressive strength to tensile strength that occurs in rock and the predicted macroscopic friction angle was much lower than the known hard rock experimental values. For this reason, several enhancements have been proposed in 2D and 3D to address these issues, namely the use of a clumped particle logic [3], the increase of the number of contacts per particle [4, 5, 6], the adoption of polygonal/polyhedral grain

structures [7, 8, 9]. With these approaches, both the biaxial failure envelope and the compressive to tensile strength ratio can be predicted. Particle models based on deformable clumped particles or polygonal particles are computationally more demanding when compared to circular or spherical particles, for this reason they have been adopted mainly in 2D models [7, 8, 10, 11].

The performance of the particle models in 2D and 3D needs to be further improved, especially in 3D, where rigid spherical particle models predict in uniaxial compression a too brittle response with two distinct slopes in the pre-peak region [5]. In the study here presented a flexible particle model is adopted that includes in an approximate way the particle deformability by considering in each grain an inner finite element mesh (triangles). The contact interaction is an extension of the rigid contact model proposed in [9].

The 2D flexible particle model is tested using biaxial tests and Brazilian tests. The results obtained are compared with those obtained with a rigid particle model with similar contact strength properties and with a flexible particle model, where the flexibility is due to the inner discretization of the grain with smaller particles. The results show that the proposed 2D flexible particle model can predict a behaviour similar to a flexible particle model through inner particle discretization that is more computationally demanding. It is also shown that when compared with a rigid model, the flexible model predicts more reasonable indirect tensile strength to direct tensile strength ratio and requires a smaller value of contact fracture energy to give a good agreement with known experimental data.

2 FORMULATION

2.1 Flexible particle model

A flexible particle model is adopted that includes in an approximate way the particle deformability by considering in each grain an inner finite element mesh (triangles). The contact interaction is an extension of the rigid contact model proposed in [9]. In order to keep the model as simple as possible, the contact between the particles is handled as if the particle is rigid and its geometry is in fact circular. Like in the rigid contact model, [9], the contact is located at the corresponding Laguerre Voronoi edge.

The inner finite element triangular mesh of each Voronoi cell is defined by a Delaunay triangulation of the Voronoi vertexes and the point corresponding to the particle centre of gravity (Figure1). The flexible contact is adopted following the contact geometry of the Voronoi tessellation. The particles are still circular but are considered to interact with neighbouring particles through the polygonal interface edges, Figure 1 a). The motion of each circular particle, representing the outer geometry of the Voronoi cell, is rigidly associated to the inner nodal point which is initially located at the particle centre of gravity.

In the flexible FEM based contact model, like in the rigid contact model [9], the contact width and the contact location are defined by the Voronoi tessellation, Figure 1 a). Like in the rigid contact model, the contact width corresponds to the length of the associated Voronoi cell edge and the contact location is also defined by the Voronoi cell edge. A scheme is then devised in order to transfer the contact forces from the contact locations to the corresponding nodal points, of the finite element mesh that represents the polygonal shaped particle, and also to properly define the contact relative velocities given the nodal velocities.

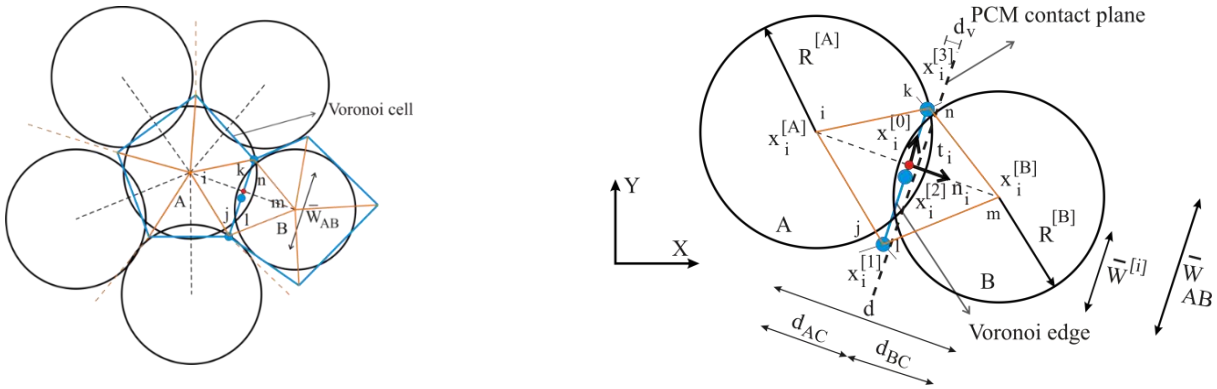

a) Contact width and location at the Voronoi cell b) 3 local contact point scheme

Figure 1: Flexible FEM based contact model for a discretization with 3 local contact points including triangular finite element mesh

The contact interaction between flexible particles follows closely the rigid contact model proposed in [9] with the exception of the contact velocity of a given local contact point, which is the velocity of particle B relative to particle A, at the contact location given by:

$$\begin{aligned} \dot{x}_i^{[J]} &= \left(\dot{x}_i^{[J]}\right)_B - \left(\dot{x}_i^{[J]}\right)_A \\ &= \left(N_{m.\Delta mnl}\dot{x}_i^{[m.\Delta mnl]} + N_{n.\Delta mnl}\dot{x}_i^{[n.\Delta mnl]} + N_{l.\Delta mnl}\dot{x}_i^{[l.\Delta mnl]}\right)_B - \\ &\quad \left(N_{i.\Delta ijk}\dot{x}_i^{[i.\Delta ijk]} + N_{j.\Delta ijk}\dot{x}_i^{[j.\Delta ijk]} + N_{k.\Delta ijk}\dot{x}_i^{[k.\Delta ijk]}\right)_A \end{aligned} \tag{1}$$

where, $N_{m.\Delta mnl}$ is the shape function value associated to nodal point "*m*" of the corresponding triangular finite element, Δ_{mnl}, at the local contact point location $\dot{x}_i^{[J]}$, and $\dot{x}_i^{[m.\Delta mnl]}$ is the velocity of nodal point "m" of the corresponding triangular plane finite element. The contact velocity is then defined using the finite element mesh discretization. As previously mentioned, the circular particles are rigidly associated to the inner nodal point that is initially located at the particle centre of gravity. The other main exception to the rigid contact model [9] is that the contact force at each local contact point needs to be transferred to the nodal points of the associated finite element triangle given the nodal shape functions. For the triangular plane finite element associated with particle A and for the triangular element associated with particle B (Figure 1b)) the local contact forces are distributed to each nodal point according to:

$$F_{i.\Delta ijk}^{c} = F_{i.\Delta ijk}^{c} - F_i^{[C]} N_{i.\Delta ijk} \tag{2}$$

$$F_{m.\Delta mnl}^{c} = F_{m.\Delta mnl}^{c} + F_i^{[C]} N_{m.\Delta mnl} \tag{3}$$

2.2 Local contact stiffness and local contact strength

The flexible model requires the user definition of the contact deformability parameters, namely the Young's modulus of the equivalent continuum material ($\bar{E}$) and the constant that

relates the normal and the shear stiffness spring value (η). In this work the local contact normal and shear stiffnesses are given by:

$$k_n^J = K_n A_c^J \tag{4}$$

$$k_s^J = \eta\, k_n^J \tag{5}$$

where, A_c^J is the contact area associated with the local point J and K_n is the normal stiffness adopted for the contact. The total contact area is given by $A_c = \overline{W}\, t$, where $\overline{W}$ is the contact interface width given by the Voronoi cell edge length, Figure 1b), and t is the out of plane thickness. For the local inter-particle contacts the flexible model also requires the definition of the contact strength properties, the maximum contact tensile stress ($\sigma_{n.t}$), the maximum contact cohesion stress (τ) and the contact frictional term (μ_c). The maximum contact local tensile strength ($F_{n.max}^{[J]}$) and the maximum local contact shear strength ($F_{s.max}^{[J]}$) are defined given the user-specified contact strength properties and the current local contact normal force ($F_n^{[J]}$) as follows:

$$F_{n.\max}^J = \sigma_{n.t}\ A_c^J \tag{6}$$

$$F_{s.\max}^J = \tau\ A_c^J + F_n^J\ \mu_c = C_{\max}^J + F_n^J\ \mu_c \tag{7}$$

where $C_{max}^{[J]}$ is the adopted maximum local contact cohesion strength. A bilinear or a brittle model under tension and shear can be adopted [9].

2.3 Model generation

The initial circular particle assembly is created by first inserting the particles with half their radius ensuring that the particles do not overlap with each other. Then the particle actual radius is adopted and a DEM cohesionless type solution is obtained, leading to a redistribution of the particle overlap throughout the assembly, Figure 2a). The particle centres of gravity are then triangulated using a weighted Delaunay scheme, Figure 2 b), and then the polygonal shaped particles are obtained given the Laguerre tessellation based on the weighted Delaunay triangulation. In each polygonal shape particle (Laguerre cell) nodal points are created at the Laguerre cell vertexes and at the particle centre of gravity. A triangulation of the nodal points of each Laguerre cell is performed, Figure 2c). Finally, the flexible contact is adopted following the contact geometry of the Voronoi tessellation. The particles are still circular but are considered to interact with the neighbouring particles through the polygonal interface edges, Figure 2d). The particle generation scheme properties are the maximum particle diameter, Dmax, the minimum particle diameter, Dmin, the radius distribution, the porosity, n, and the particles density, ρ. In the simulations that were carried out, a porosity value of 10% was adopted in the definition of the initial number of particles to be inserted [1, 2]. Figure 2c) and Figure 2d) show that the adopted scheme generates a compact flexible particle assembly with polygonal edge interactions that has no porosity.

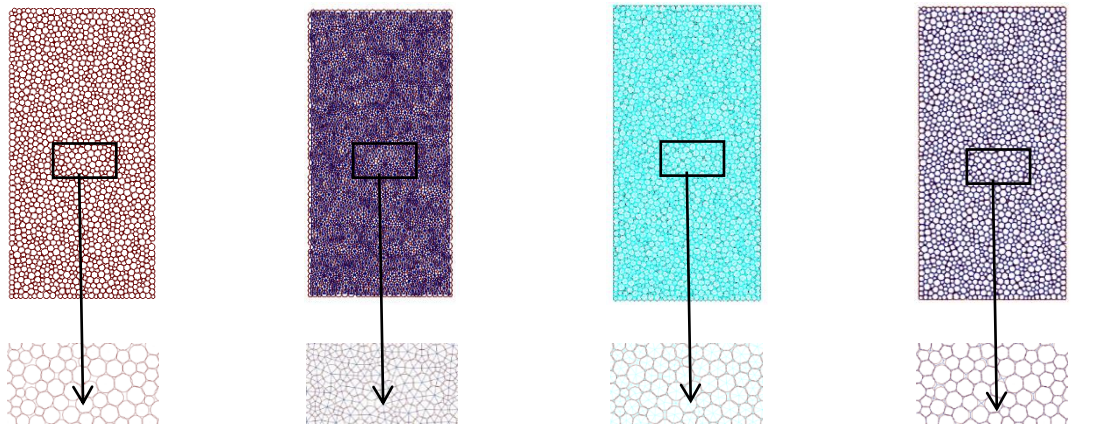

a) Grain structure | b) Flexible contact connection | c) Flexible inner triangular plane elements mesh | d) Flexible contact width

Figure 2: From the grain structure to the flexible contact including plane element mesh

3 BIAXIAL AND BRAZILIAN TESTS IN A GRANITE ROCK

3.1 Numerical setup

The flexible FEM based particle model is validated against known uniaxial, biaxial and Brazilian tests in a granite rock [7]. The uniaxial tests, without lateral confinement pressure, and the biaxial tests with lateral confinement pressure are performed in samples with 80 mm × 160 mm. The Brazilian tests are performed on circles with a diameter of 80 mm. The simulations are performed in 2D, therefore the particle assembly is considered to have 80 mm thickness. The course aggregate of Augig granite ranges from 3.0 to 7.0 mm [7]. In order to simulate this rock, both geometries where discretized with particles with a uniform diameter distribution ranging from 3.0 to 5.0 mm.

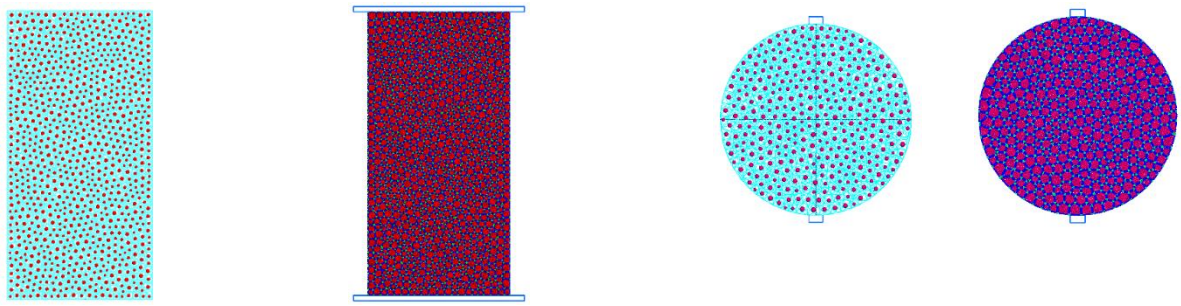

a) Uniaxial test (tensile and compression) and biaxial test – FEM based | b) Uniaxial test (tensile and compression) and biaxial test – FEM based | c) Brazilian test – FEM based | d) Brazilian test – DEM based

Figure 3: Flexible particle model assemblies

The uniaxial tests and the biaxial tests with lateral confinement have in average 920 particles, 10488 nodes, 13892 triangular finite elements and 2561 contacts with 3 local points Figure 3a), the Brazilian tests have in average 360 particles, 4106 nodes, 5439 triangular finite elements and 997 contacts with 3 local points Figure 3c). Particle assemblies where the grain

deformability is defined through the inner contacts were also created, the uniaxial tests have in average 42699 particles, and 117944 contacts with 1 local point Figure 3a), the Brazilian tests have in average 16800 particles and 46243 contacts with 3 local points, Figure 3c). For the inner grain discretization an average particle diameter of 0.05 mm was adopted.

3.2 Deformability

Several parametric studies were carried in order to assess the influence of the contact elastic parameters and of the elastic parameters adopted in the finite element mesh on the macroscopic particle assembly elastic response, given by its Young's modulus (E) and Poisson's coefficient (υ). For the flexible particle assemblies based on FEM discretization two different values of the Young's modulus were adopted, a value of 25.8 GPa similar to the Young´s modulus of Augig granite and a value of 51.6 GPa in the order of magnitude of the Young´s modulus of the minerals usually present in a granite rock. A Poisson's coefficient of 0.23 similar to the known Poisson´s coefficient of an Augig rock was adopted.

Figure 4a) shows that in the rigid contact model [9] both contact elastic parameters influence the macroscopic Young's modulus of the particle assembly, It is also shown that the macroscopic Young's modulus is more sensitive to the shear to normal stiffness ratio for higher K_n values. Figure 4b) shows that in the rigid contact model the macroscopic Poisson's coefficient is mainly influenced by the shear to normal stiffness relationship (η). The dashed line represents the known values for an Augig rock (E=23.8 GPa, u= 0.23).

Figure 4c) and Figure 4d) show the macroscopic elastic response, Young's modulus and Poisson's coefficient, obtained with the flexible particle model when it is assumed, for the inner triangular elements elements, a Young´s modulus in the order of magnitude of the minerals that are present in a granite rock, (e.g. quartz). When compared with the rigid model, in the flexible particle model the parameter η has a smaller effect in the macroscopic Young's modulus, as the macroscopic particle assembly deformability is mostly influenced by the elastic parameters adopted for the inner finite element mesh.

Figure 4e) and Figure 4f) show the macroscopic elastic response, Young's modulus and Poisson's coefficient, obtained with the flexible particle model using for the inner triangular finite elements a Young´s modulus equal to that of an Augig rock. In this approach, the contact normal stiffness influence and the parameter η influence is almost negligible. In the latter case the contact stiffness needs to be set to a higher value as the deformability should be only due to the inner triangular mesh deformation. As shown in Figure 4b), 4d) and 4e) the adoption of a flexible particle model greatly reduces the restrictions in the values adopted for the parameter η, whereas in a rigid particle model this term is essential in order to obtain the correct macroscopic Poisson´s ratio.

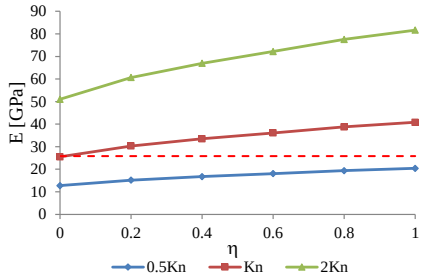

a) Rigid contact model [9]: Macroscopic Young's modulus for varying η - K_n = 1x10^4 GPa/m

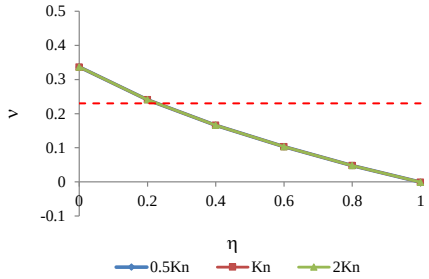

b) Rigid contact model [9]: Macroscopic Poisson's coefficient for varying η - K_n = 1x10^4 GPa/m

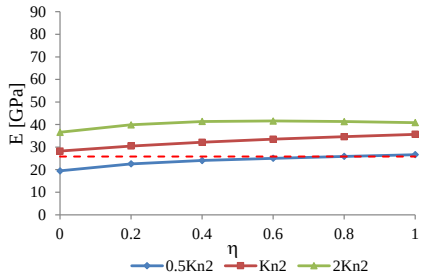

c) Flexible particle model: Macroscopic Young's modulus for varying η - K_n = 2.5x10^4 GPa/m, E = 51.6 GPa

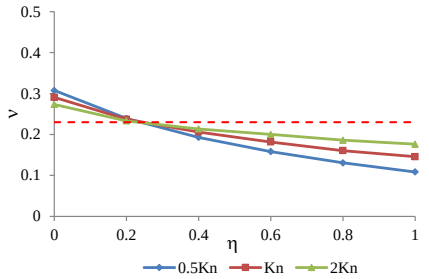

d) Flexible particle model: Macroscopic Poisson's coefficient for varying η - K_n = 2.5x10^4 GPa/m, E = 51.6 GPa

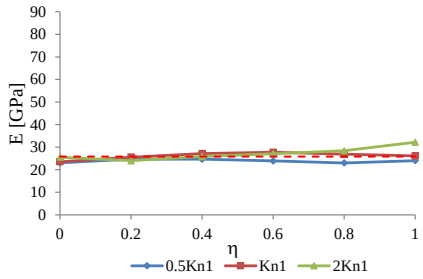

e) Flexible particle model: Macroscopic Young's modulus for varying η - K_n = 15.0x10^4 GPa/m, E = 25.8 GPa

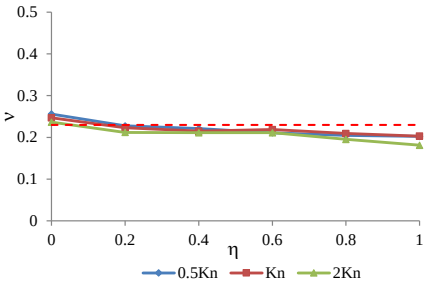

f) Flexible particle model: Macroscopic Poisson's coefficient for varying η - K_n = 15.0x10^4 GPa/m, E = 25.8 GPa

Figure 4: Influence of the contact deformability parameters (K_n and η) on the elastic macroscopic properties of the particle assembly (E and υ) for the rigid contact model [9] and for the flexible FEM based particle model for two different finite element Young´s modulus values

3.2 FEM versus DEM deformability

Figure 5 shows the crack patterns obtained in uniaxial compression, direct tensile and in an indirect tensile test for the rigid particle model [9], for a flexible particle model based on a triangular FEM discretization and for a flexible particle model where the grain deformability is due to the inner discretization of the grains with smaller particles. The crack patterns obtained for the different tests are accordingly to those expected. Figure 5 shows that there are similarities in the final predicted crack patterns when the grain deformability is taken into account, either through finite elements or through smaller particle discretization.

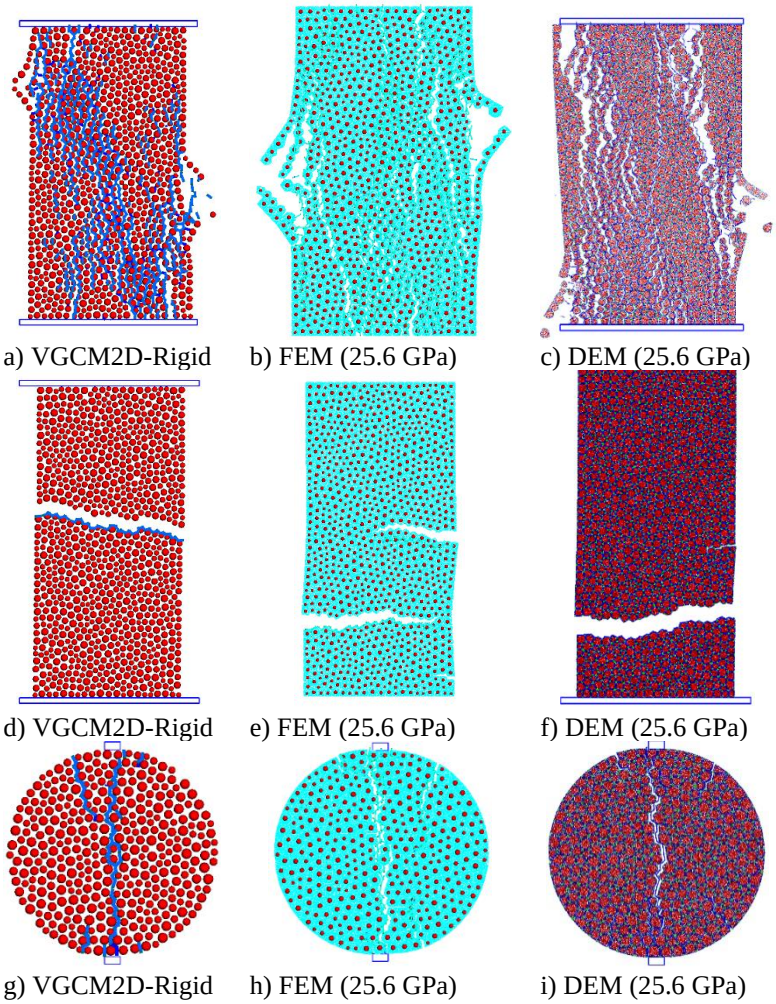

Figure 5: Bilinear contact model – Predicted failure patterns

Figure 6 shows the axial stress-displacement response under compression, including the contact damage evolution for the rigid particle model, for the FEM based deformable particle model and for two DEM based deformable particle models, one where the unit contact normal at the grain boundaries is given by the Voronoi cell edge contact normal (DEM-un) and another model where the contact normal is defined using the usual formula (DEM) [1, 2]. It can be seen that the FEM based deformable model is close to the DEM-un deformable model in terms of stress-displacement relationship and contact damage evolution.

Figure 6 also shows the influence of the adopted grain roughness on the post-peak response and on the obtained maximum compression strength, showing that the particle size adopted in the inner grain discretization merits special attention in order to reduce this effect or by setting the contact normal to the initial grain boundary edge.

The computational run times associated with the VGCM2D-Flexible contact model are higher than those associated with the rigid version, with an average multiplying factor of 8.0, but smaller than the computational run times associated with the DEM deformable model which are 30 times higher than those of the rigid version.

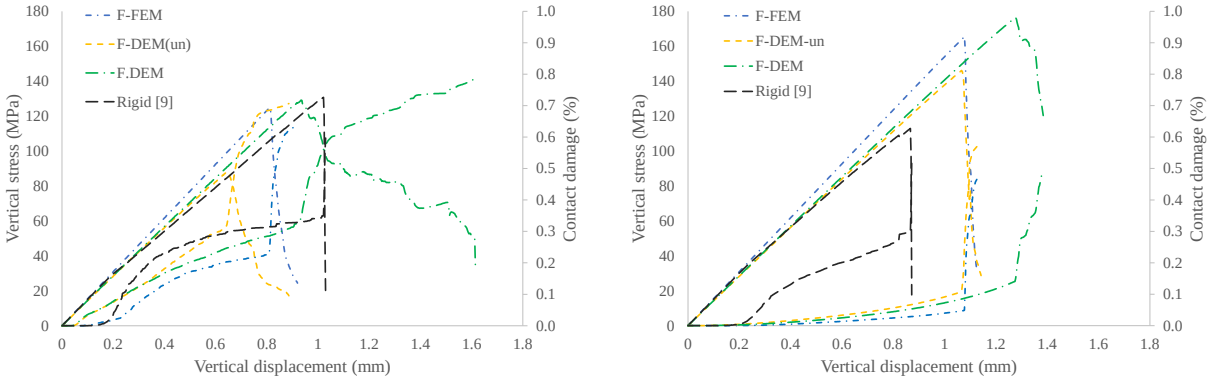

a) Brittle b) Bilinear softening

Figure 6: Axial stress-displacement response under uniaxial compression: Brittle and Bilinear numerical responses - Rigid model [9] and flexible particle models (FEM, DEM)

3.3 Strength envelope

Table 1 presents the micromechanical elastic and strength properties that were adopted for the numerical analyses that were carried out. The adopted strength values were similar to those adopted previously for a rigid contact model [9], that were found to predict numerical results closer to the experimental data of an Augig granite rock [7]. The Augig granite macro-properties presented in [7] are shown in Table 2, along with the obtained numerical responses.

Table 1: Elastic and strength particle model properties

a) Elastic contacts and inner elements

	K_n (GPa/m)	η	E (GPa)	n
Rigid [9]	0,83x10^4	0.235	-	-
FEM-E=25.8 GPa	20,0x10^4	0.235	25.8	0.23

b) Strength contact properties

	μ_c	$\sigma_{n.t}$ [MPa]	τ [MPa]	$G_{f,n}$ [N/m]	$G_{f,s}$ [N/m]
Brittle model	0.40	13.7	48.8	-	-
Bilinear contact model	0.50	11.5	33.25	66.1	2078.7

Figure 7 shows the Hoek-Brown failure criterion applied to the Augig granite experimental values [7] and the values predicted adopting both the flexible FEM based model and using a rigid contact model [9]. Brittle and bilinear softening contact laws were adopted in each particle model. The flexible particle model following a brittle constitutive law predicts an indirect tensile strength of the same magnitude of the direct tensile strength, contrary to the tensile strength values predicted with a rigid model. It can also be seen that a flexible particle model with a brittle constitutive law predicts a higher friction coefficient for higher lateral confinement values. This can be explained by the fact that with a flexible contact model the local contact points inter particle distance at failure is much closer than the local points inter-particle distance at failure with a rigid brittle model, because in the latter the contact normal

stiffness is lower as it also needs to represent the overall particle assembly deformability.

When adopting a bilinear model it can be seen that flexible models predict an indirect tensile strength higher that the direct tensile strength, whereas with a rigid model predicts an indirect tensile strength of the same order of magnitude of the direct tensile strength. It can also be seen that with the flexible particle model a higher cohesion and a slightly higher friction angle are predicted with a bilinear constitutive law, see also Table 2.

Table 2: Augig granite macro-properties (Experimental and Numerical).

	σ_c (MPa)	$\sigma_{t.dir}$ (MPa)	$\sigma_{t.ind}$ (MPa)	c (MPa)	ϕ (^{o})
Augig granite [7]	122.1	-	8.8	21.0	53.0
Rigid [9]-Brittle	130.8	7.8	5.3	24.8	48.5
FEM (25.6 GPa)-Brittle	125.0	7.4	8.0	19.4	55.5
Rigid [9]-Bilinear	112.9	8.6	7.9	22.4	46.7
FEM (25.6 GPa)-Bilinear	165.5	11.4	15.2	28.5	52.0

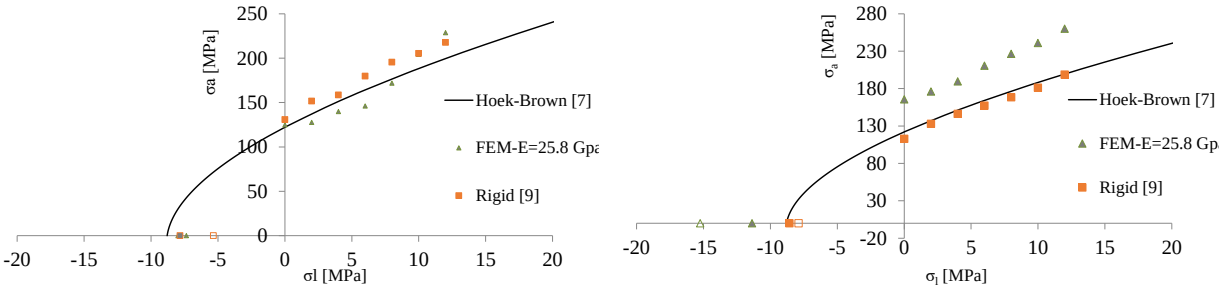

a) Brittle contact constitutive law b) Bilinear softening contact constitutive law

Figure 7: Strength envelope: Hoek-Brown failure criterion [7], rigid model [9] and flexible FEM based particle model

Figure 8 shows the axial stress-displacement response for the flexible particle model and for the rigid contact model [9], for a brittle contact law and for a bilinear softening contact law, adopting similar contact strength values. It is shown that with a flexible particle model, and for higher lateral confinement a small yield plateau can be identified, whereas in the rigid model this effect occurs only for higher confinement values and for the bilinear contact model. It can also be seen that for low lateral confinement values, the post-peak response predicted with a flexible particle model is more ductile. The higher ductility that occurs in the rigid particle model for higher lateral confinements is mostly due to the fact that, for computational reasons, a coarse particle assembly was adopted.

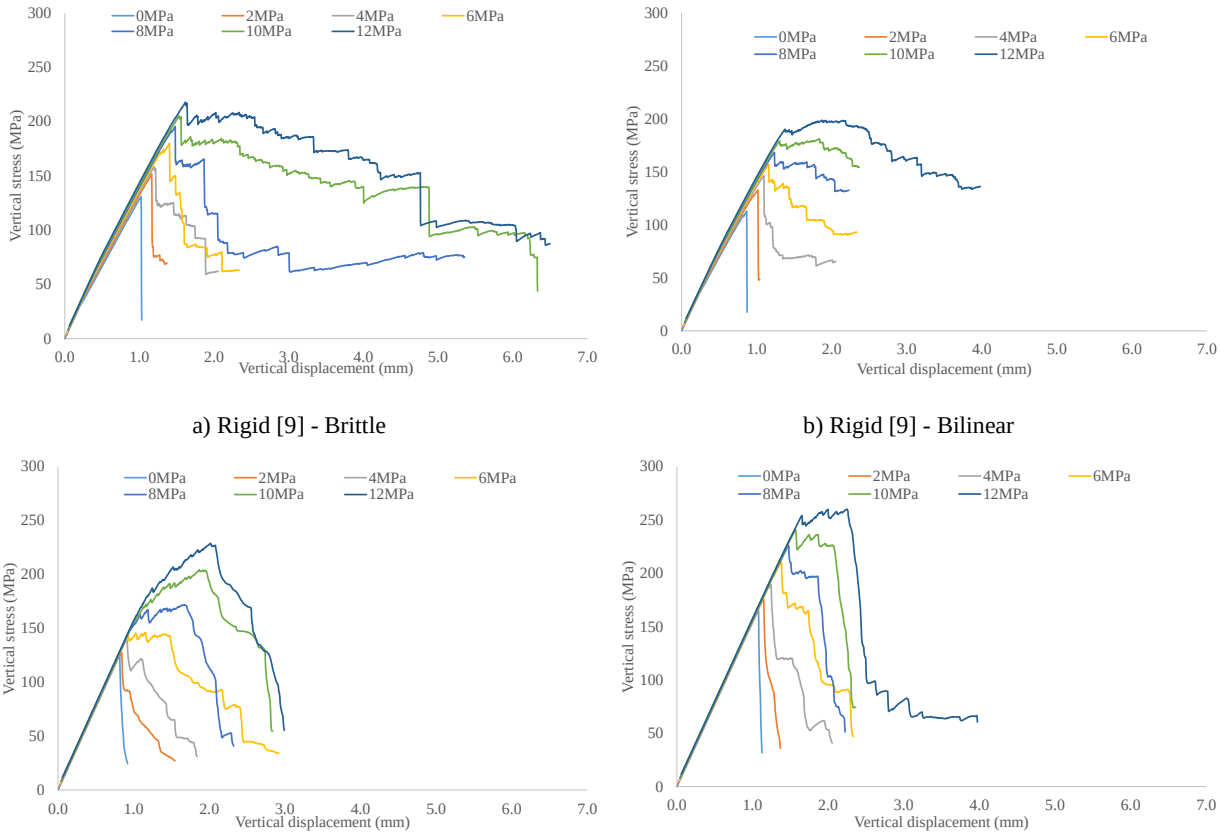

a) Rigid [9] - Brittle

b) Rigid [9] - Bilinear

c) FEM (E=25.6MPa) - Brittle

d) FEM (E=25.6MPa) - Bilinear

Figure 8: Axial stress-displacement response: Brittle and Bilinear numerical responses - Rigid contact model [9] and flexible FEM based particle model

4 CONCLUSIONS

A flexible particle based on FEM discretization, which enables moment transmission and contact discretizations with multiple local contact points is shown to predict a response in close agreement with a flexible particle DEM based model. It is shown that the execution times of the flexible particle model are around 4 times lower than the execution times of a similar DEM based flexible particle model. The results presented show that in a DEM based flexible particle model it is important to adopt a smaller particle discretization or a contact normal defined by the grain boundaries in order to reduce the grain roughness effect.

The adoption of a flexible particle model greatly reduces the restrictions in the values adopted for the parameter that relates the normal to shear contact stiffnesses, , whereas in a rigid particle model this term is essential in order to obtain the correct macroscopic Poisson´s ratio. It is shown that the particle deformability influences the indirect tensile strength to direct tensile strength ratio, for both brittle and bilinear contact models. It is known that rigid particle models require higher fracture energies in order to be able to predict a indirect tensile strength ratio higher that the direct tensile strength vale. The results presented show that a flexible particle model requires, when compared with a rigid model, a smaller value of contact fracture energy in order to give a good agreement with known experimental data.

ACKNOWLEDGMENTS

The study presented here is part of the research project "DAMFA: Cutting-edge solutions for sustainable assessment of concrete dam foundations" which has been supported by LNEC with the main purpose of developing a numerical multiphysic integrated tool for the sustainable assessment of concrete dam foundations, taking into account the interaction between the mechanical, hydraulic and thermal behaviours.

REFERENCES

[1] Potyondy, D., Cundall, P. and Lee C. *Modelling rock using bonded assemblies of circular particles*. In: Aubertin M. et al (eds) Proceedings of the 2nd North American Rock Mechanics Symposium, Rotterdam, Balkema, (1996), 1937-1944.

[2] Potyondy, D. and Cundall, P. A bonded-particle model for rock. *International Journal of Rock mechanics and Mining Sciences* (2004) 41(8): 1329-1364.

[3] Cho N, Martin C, Sego DC (2007) A clumped particle model for rock. *International Journal of Rock mechanics and Mining Sciences* 44(7):997-1010.

[4] Wang, Y. and Tonon, F. Modeling Lac du Bonnet granite using a discrete element model. International Journal of Rock mechanics and Mining Sciences (2009), 46(7): 1124:1135.

[5] Monteiro Azevedo, N. and Lemos, J. A 3D generalized rigid particle contact model for rock fracture. Engineering Computations (2013), 30(2):277-300.

[6] Scholtès, L. and Donzé, F.V. A DEM model for soft and hard rocks: Role of grain interlocking on strength. *Journal of the Mechanics and Physics of Solids* (2013), 61(2):352-369.

[7] Kazerani, T. and Zhao, J. Micromechanical parameters in bonded particle method for modelling of brittle material failure, *International Journal for Numerical and Analytical Methods in Geomechanics*, (2010), 34(18):1877-1895.

[8] Lan H, Martin C, Hu B, Effect of heterogeneity of brittle rock on micromechanical extensile behaviour during compression loading. *Journal of Geophysical Research* (2010) 115(B1):1-14.

[9] Monteiro Azevedo, N., Candeias, M. and Gouveia, F., A rigid particle model for rock fracture following the Voronoi tessellation of the grain structure: Formulation and Validation, *Rock mechanics and Rock Engineering*, (2015), 48(2):535-557.

[10] Gao, F. and Stead, D., The application of a modified Voronoi logic to brittle fracture modelling at the laboratory and field scale. *International Journal of Rock Mechanics and Mining Sciences,* (2014), **68**: 1-14.

[11] Ghazvinian, E., Diederichs, M. and Quey, R., 3D Random Voronoi grain-based models for simulation of brittle rock damage and fabric-guided micro-fracturing. *Journal of Rock Mechanics and Geotechnical Engineering*, (2014), **6(6)**: 506:521.